Supporting Information

Rapidly Synthesized Porous Alloy Heterostructure Catalyst for Ultra-Low Energy Water Splitting under Industrial Conditions

Yan Wang [a], Feng Chen [a], Zikang Zhao [a], Ying Zhang [a], Shengwei Sun [a], Shan Song [a], Tianshuo Wang [a], Yubin Yuan [a], Junshuang Zhou [a,*], Faming Gao [a,b,*]

[a] Hebei Key Laboratory of Applied Chemistry, School of Environmental and Chemical Engineering, State Key Laboratory of Metastable Materials Science and Technology, Yanshan University Qinhuangdao 066004 (China)

[b] Tianjin Key Laboratory of Multiplexed Identification for Port Hazardous Chemicals, Tianjin University of Science and Technology, Tianjin 300457, China

[*]Corresponding author. E-mail: fmgao@ysu.edu.cn; jszhou@ysu.edu.cn;

1. Experimental Procedures

Reagents and chemicals: 2 mm thick Raney nickel was purchased from Ying kai mo Metal Mesh Limited; Hydrochloric acid (hydrochloric acid, AR, 38%) was purchased from Xilong Chemical Co., Ltd.; ethanol (C_2H_5OH, AR, 98%), nickel chloride hexahydrate ($NiCl_2 \cdot 6H_2O$, AR, 98%); Potassium hydroxide (KOH, AR, 85%), ferrous chloride ($FeCl_2$) were purchased from Kaitong Chemical Reagent Co., Ltd.; Sodium acetate (sodium acetate) was purchased from Leader Pharmaceutical Technology Co., Ltd.

Energy consumption calculations： The calculation and formula of the energy efficiency production capacity of hydrogen production by water electrolysis are explained in the energy efficiency limit value and energy efficiency class of the water electrolysis hydrogen production system (GB-32311-2015). We can calculate the gas production of the electrolyzer according to this or design the number of chambers of the electrolyzer according to the gas production, etc.: in the standard state, with 2×96500 C of electricity, 1 mol H_2O can be electrolyzed to produce 1 mol H_2 and 0.5 mol O_2, and the volume of 1 mol H_2 in the standard state is 22.43×10^{-3} m^3.

$2\times96500\times1000 / (3600\times22.43)=2390$ A h m^{-3}

Current test values are calculated by the formula for gas production:

$Q=I\ n\ \eta_0 / 2390$

Where:

Q: Hydrogen production in cubic meters per hour (m^3 h^{-1});

I: DC power supply through the chamber of the water electrolyzer, in amperes (A);

n: The number of electrolysis cells;

η_0: Current efficiency, programmable to 100%

$P=U\ I$

$W=P\ t=U\ I\ t$ unit: Kw h

U: The voltage corresponding to different current densities

I: The amount of current corresponding to different current densities

t: Time should be 1 h

Energy consumption=W / Q   Unit: Kw h/N m^3 H_2

Supplementary Figures

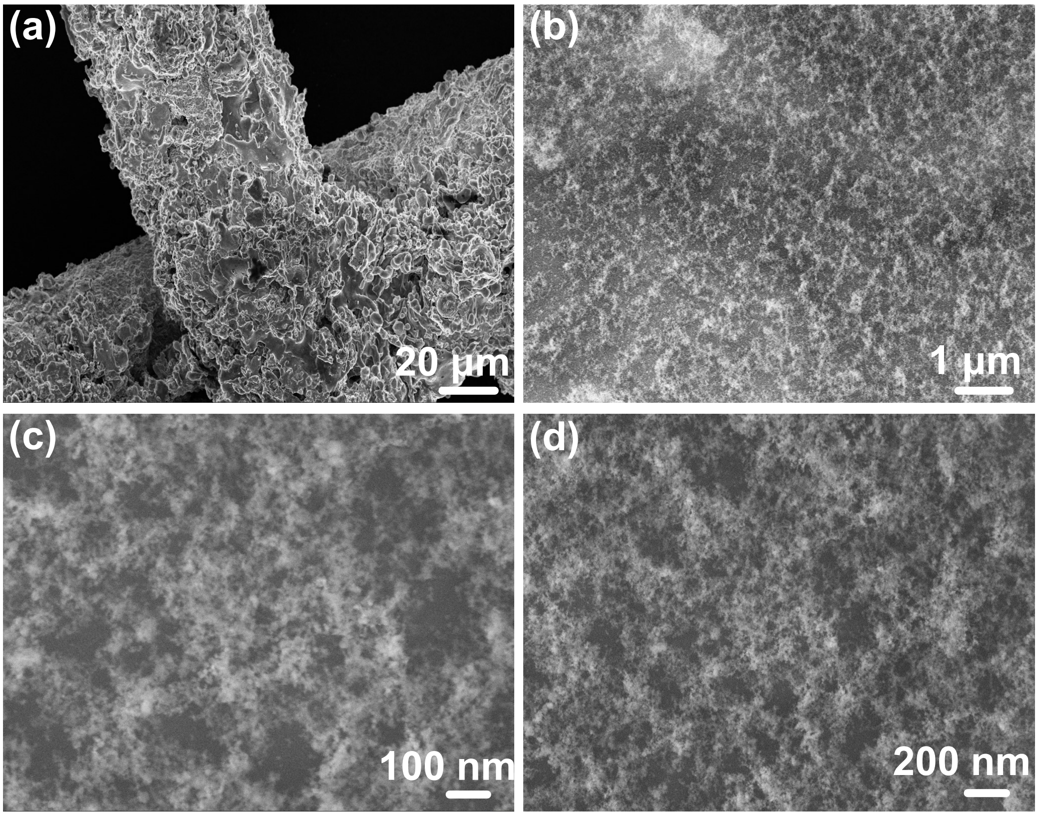

Figure S1. Low and high magnification SEM images of porous RN at (a) 20 µm, (b) 1 µm, (c) 100 nm, and (d) 200 nm.

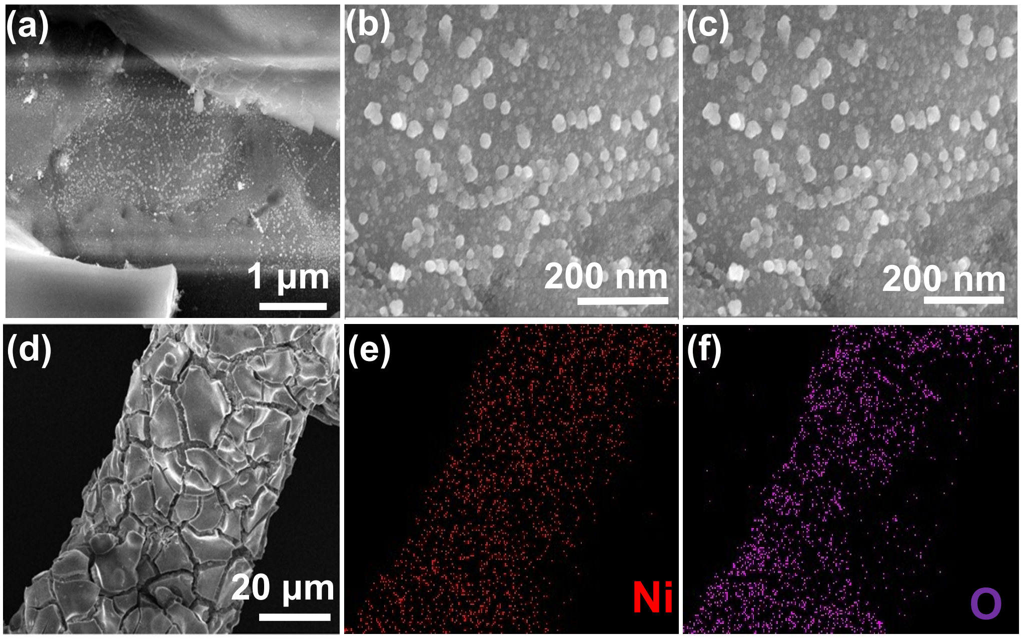

Figure S2. SEM images of the Ni@RN catalyst at (a) 1 μm, (b) 20 nm, (c) 200 nm, and (d) 20 μm; EDS elemental mapping images of the Ni@RN catalyst (e) Ni and (f) O.

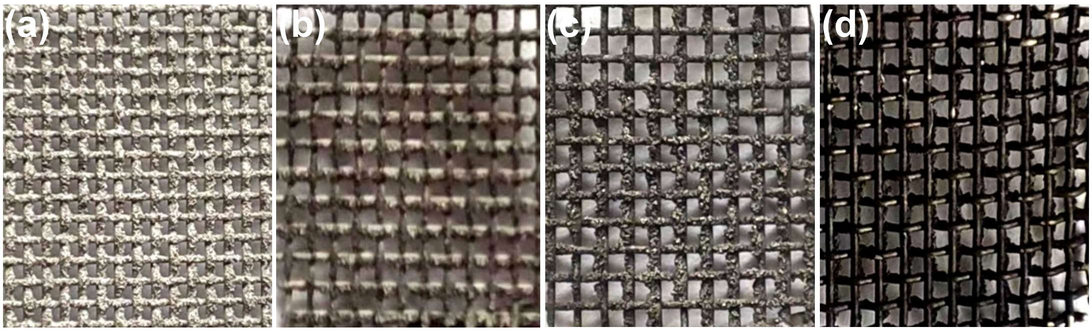

Figure S3. Optical images of different electrodeposition currents. (a) 30 mA; (b) 60 mA; (c) 90 mA and (d) 120mA.

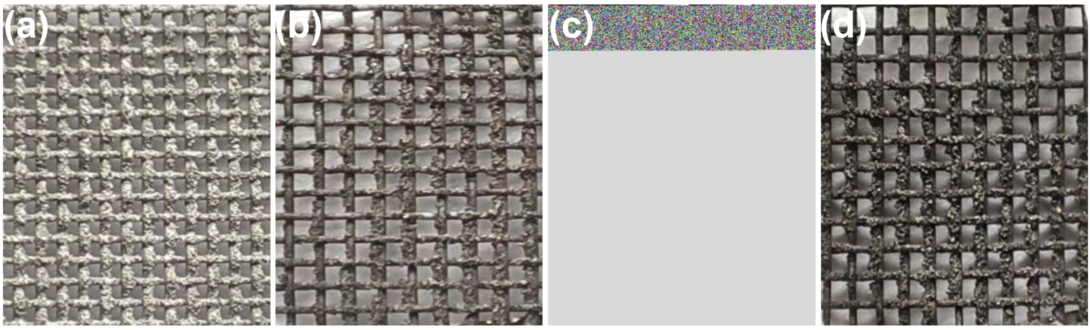

Figure S4. Optical images of different electrodeposition times. (a) 1 min; (b) 3 min; (c) 10 min and (d) 12 min.

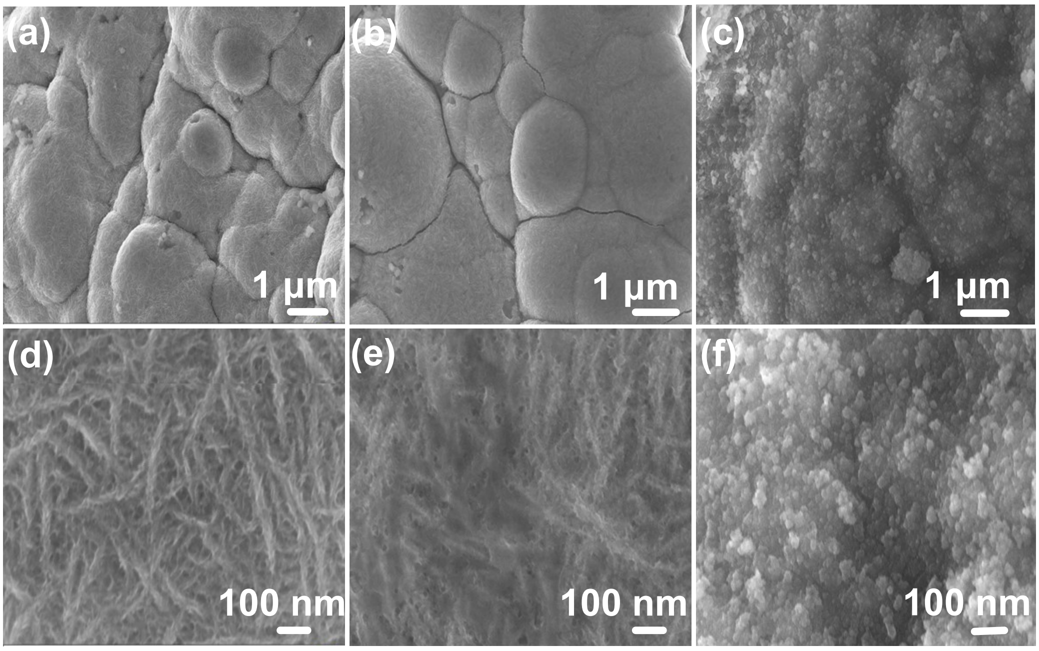

Figure S5. Low and high magnification SEM images of NiFe@RN that synthesize at a different electrodeposition current. (a and d) 30 mA; (b and e) 60 mA and (c and f) 120 mA.

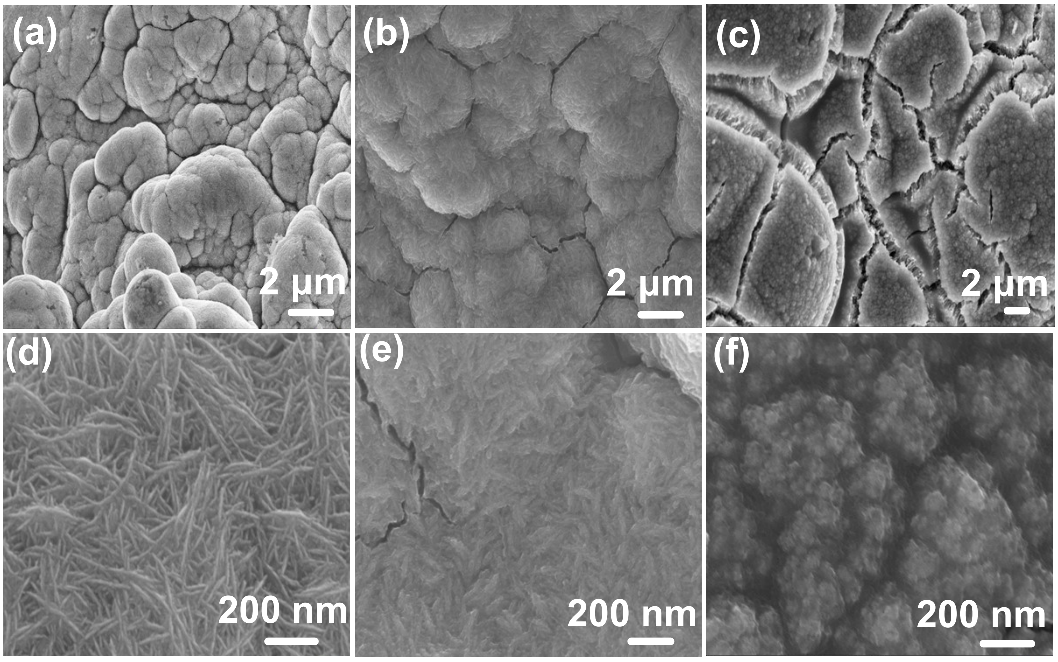

Figure S6. Low and high magnification SEM images of NiFe@RN that synthesize at a different electrodeposition time (a and d) 1 min; (b and e) 3 min and (c and f) 12 min.

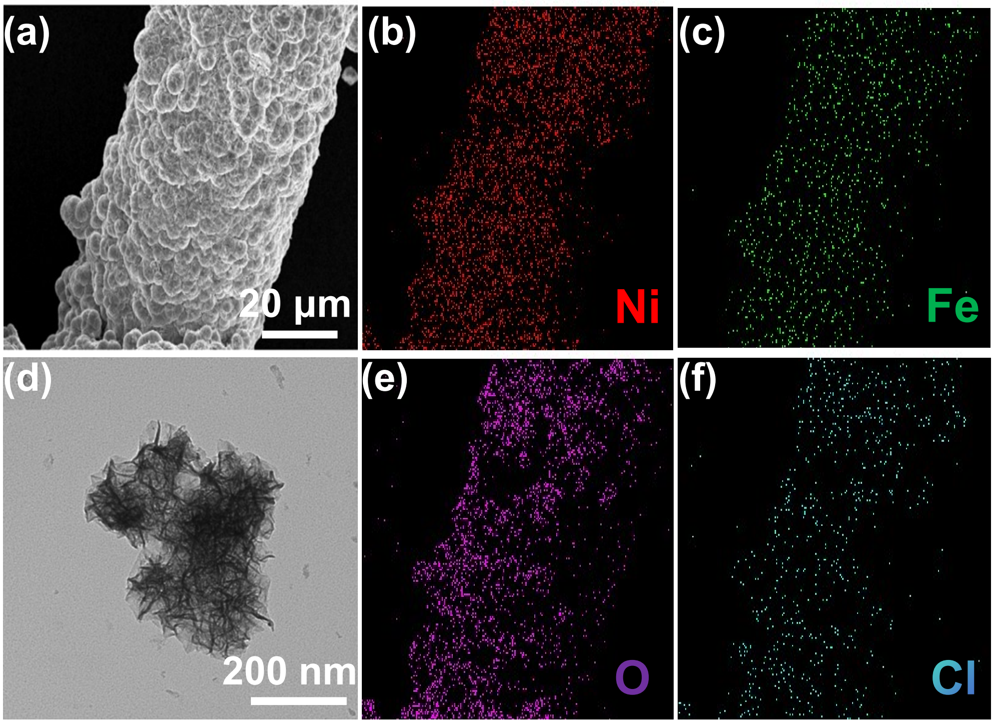

Figure S7. SEM images of the NiFe@RN catalyst at (a) 20 μm; TEM image of the NiFe@RN catalyst (200 nm) at (d); EDS elemental mapping images of the NiFe@RN catalyst (b) Ni ; (c) Fe; (e) O and (f) Cl.

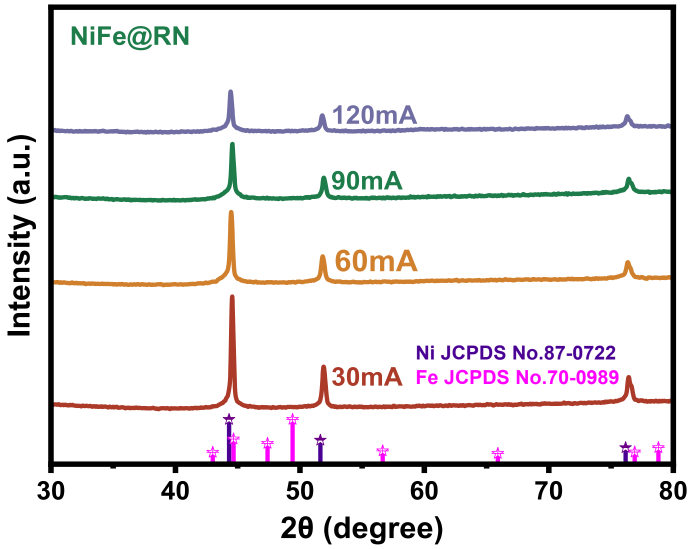

Fig S8. X-ray diffraction patterns of NiFe@RN catalyst that synthesize at a different electrodeposition current (30 mA, 60 mA, 90 mA, and 120 mA).

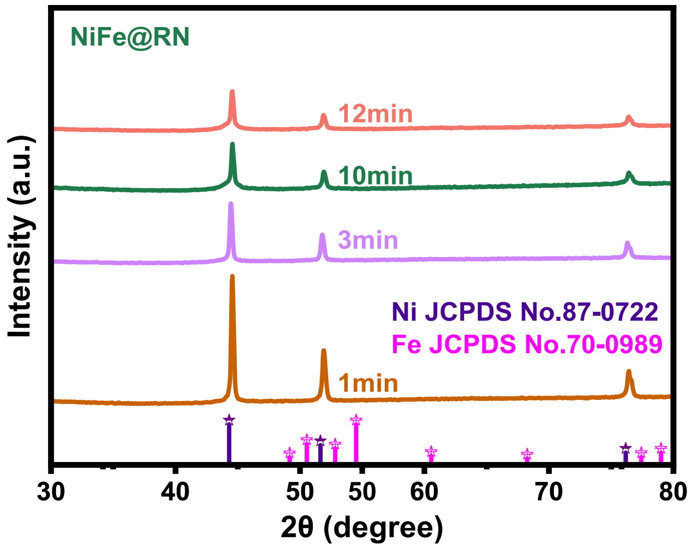

Fig S9. X-ray diffraction patterns of NiFe@RN catalyst that synthesize at a different electrodeposition time (1 min, 3 min, 10 min, and 12 min).

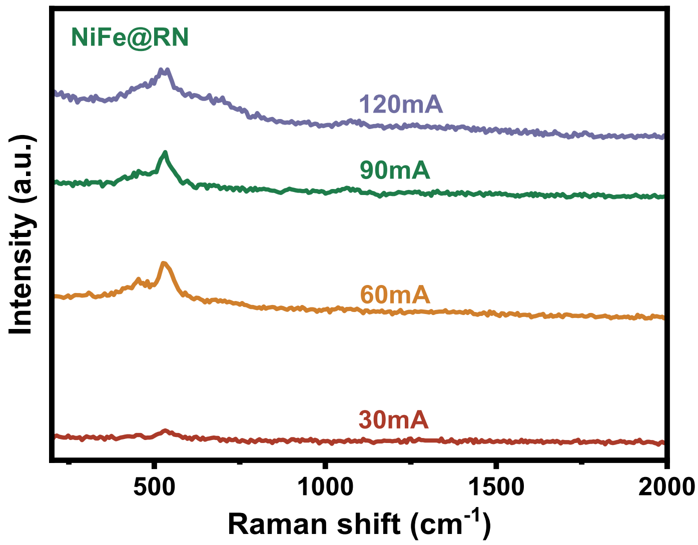

Fig S10. Raman spectra of NiFe@RN catalyst that synthesize at a different electrodeposition current (30 mA, 60 mA, 90 mA, and 120 mA).

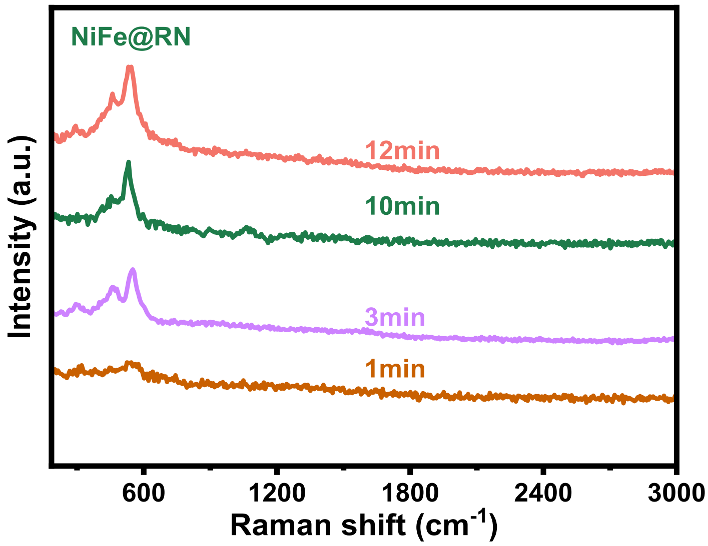

Fig S11. Raman spectra of NiFe@RN catalyst that synthesize at a different electrodeposition time (1 min, 3 min, 10 min, and 12 min).

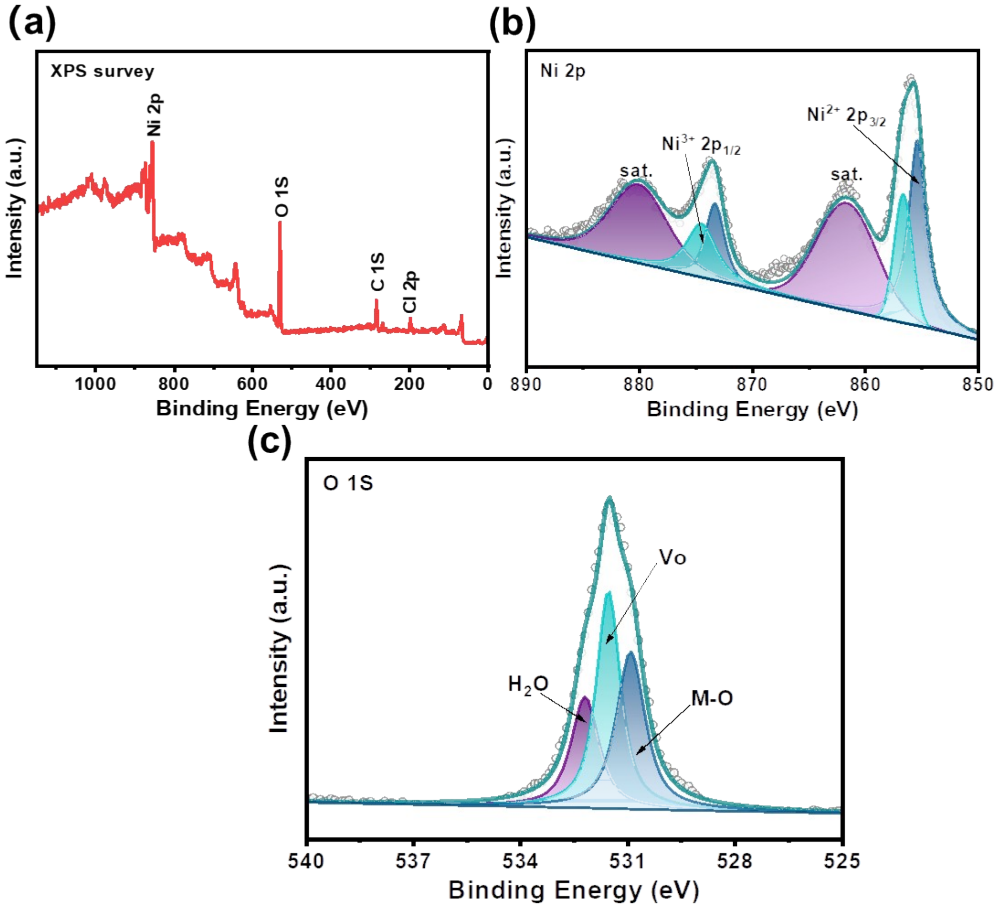

Fig S12. XPS spectra of Ni@RN electrode (a) XPS total spectrum; (b) Ni 2p plot; (c) O 1s plot.

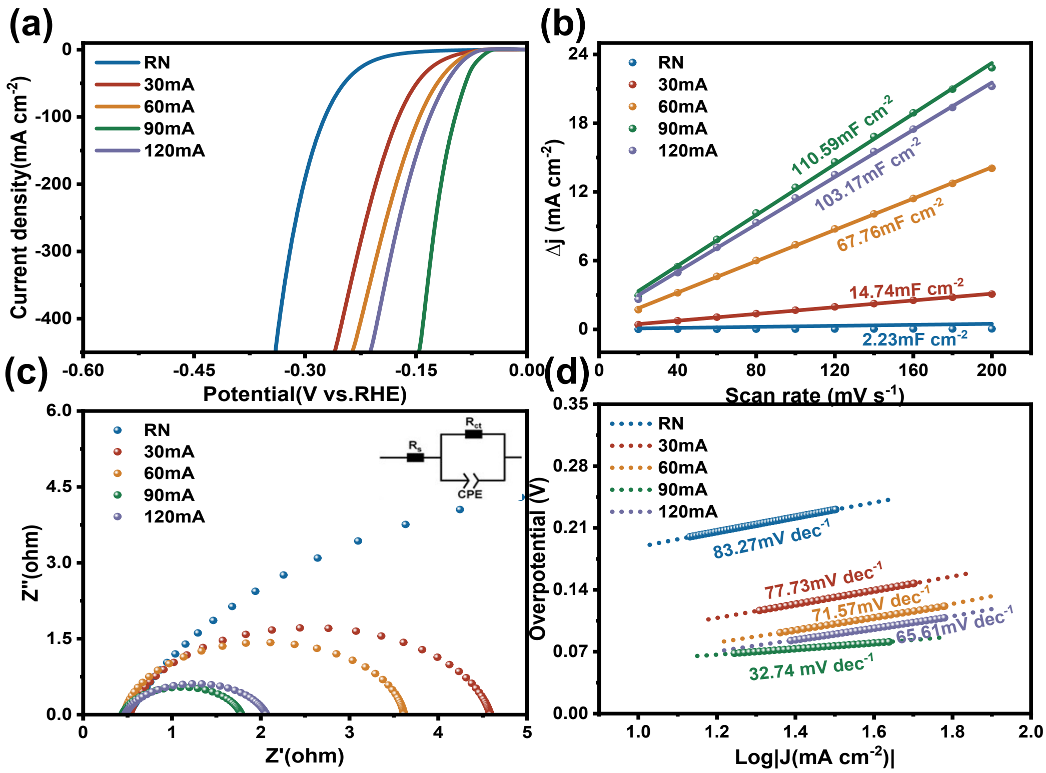

Fig. S13. (a) LSV curve of NiFe@RN HER catalyst that synthesizes at a different electrodeposition current in 6 M KOH solution, with a scanning rate of 1 mV s^{-1}; (b) Cdl calculation; (c) Electrochemical impedance spectroscopy (EIS) plots; (d) Tafel slope.

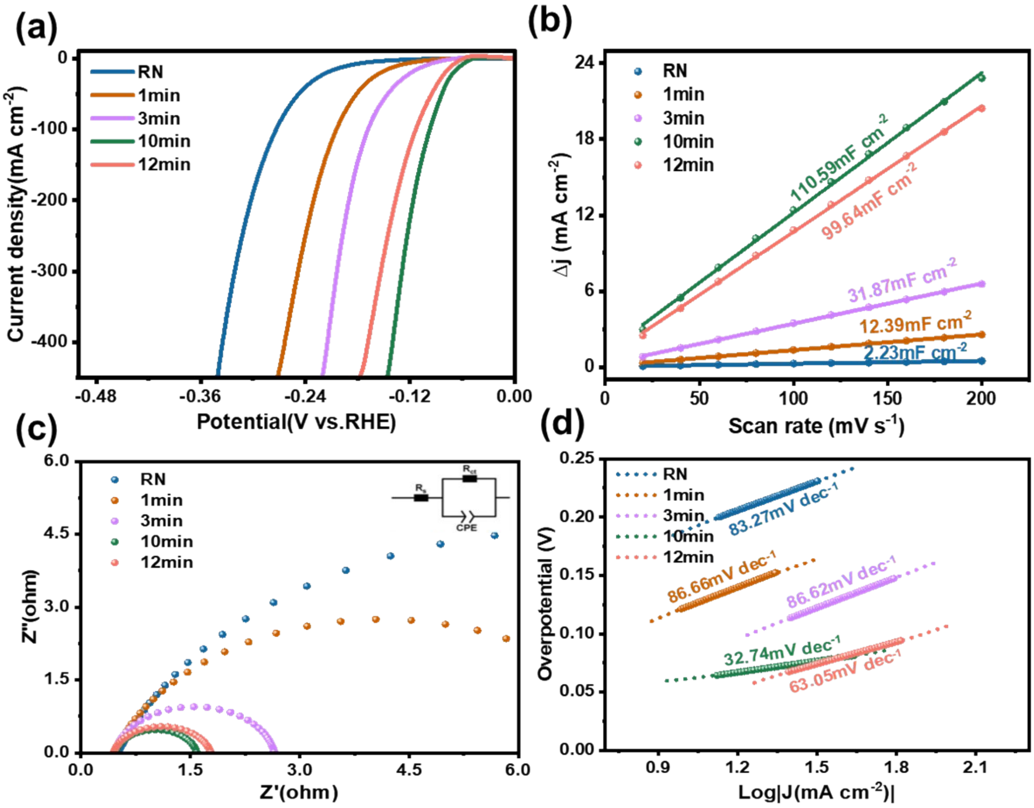

Fig. S14. (a) LSV curve of NiFe@RN HER catalyst that synthesizes at a different electrodeposition time in 6 M KOH solution, with a scanning rate of 1 mV s^{-1}; (b) Cdl calculation; (c) Electrochemical impedance spectroscopy (EIS) plots; (d) Tafel slope.

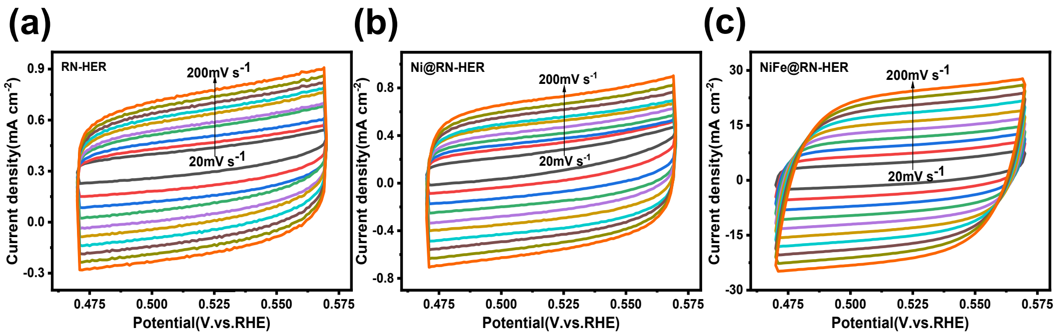

Fig S15. CV diagram (0.47-0.57 mV) of HER catalyst in 6 M KOH electrolyte. (a) RN; (b) Ni@RN and (c) NiFe@RN.

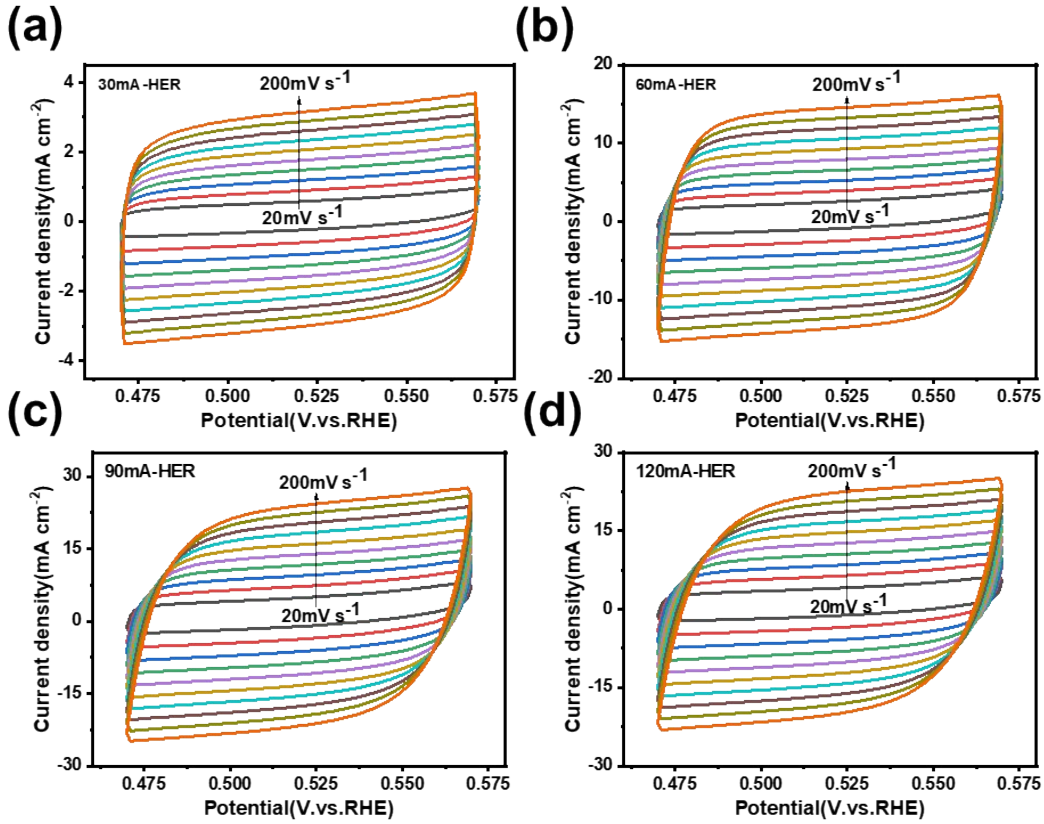

Fig S16. CV diagram (0.47-0.57 mV) of NiFe@RN HER catalyst that synthesizes at a different electrodeposition current. (a) 30 mA; (b) 60 mA; (c) 90 mA and (d) 120 mA.

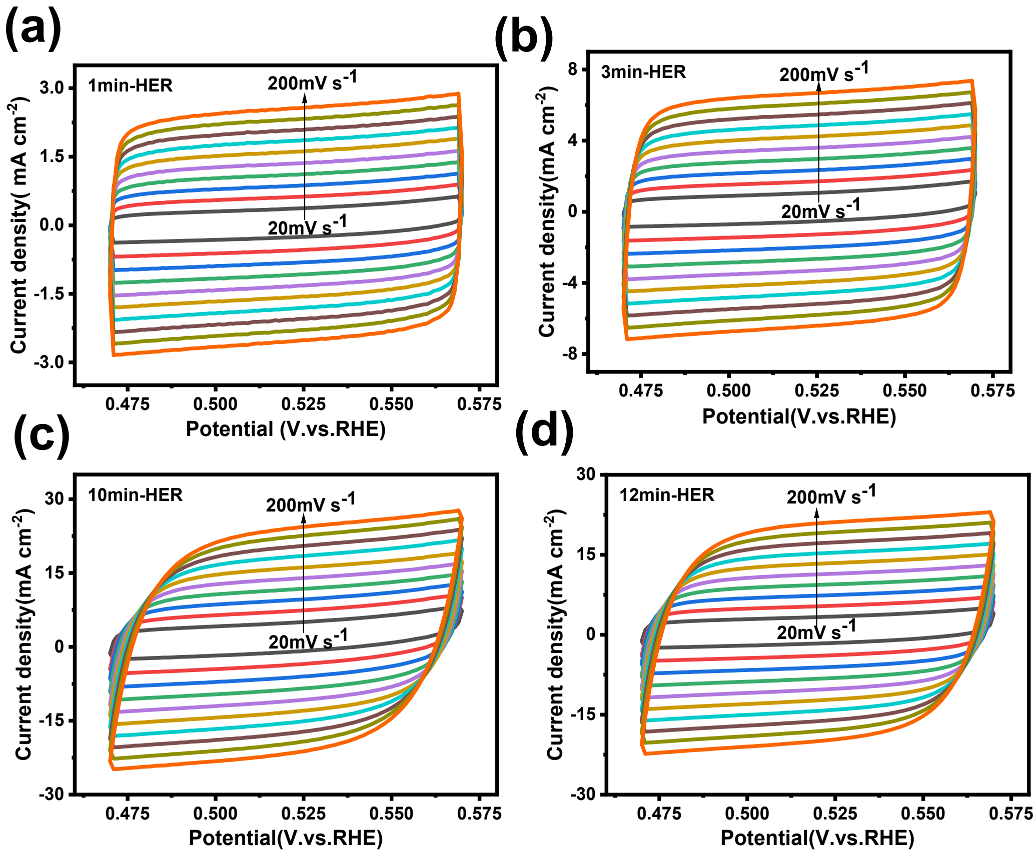

Fig S17. CV diagram (0.47-0.57 mV) of NiFe@RN HER catalyst that synthesizes at a different electrodeposition current. (a) 1 min; (b) 3 min; (c) 10 min and (d) 12 min.

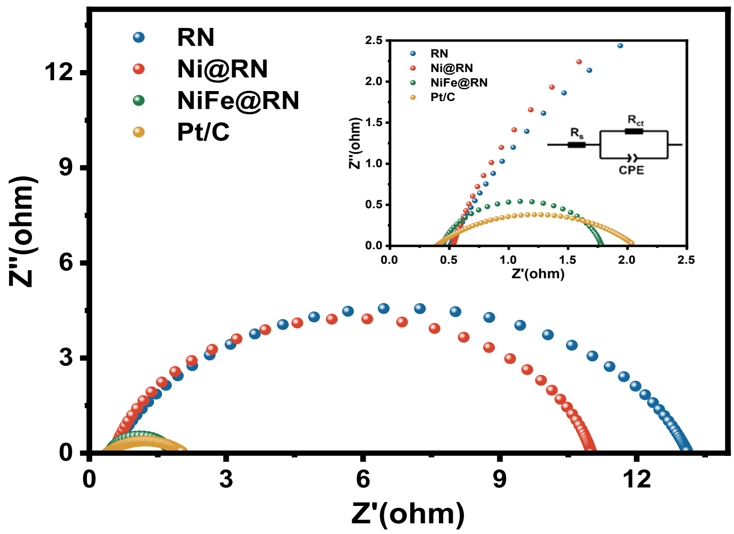

Fig S18. Nyquist plots of NiFe@RN and other catalysts.

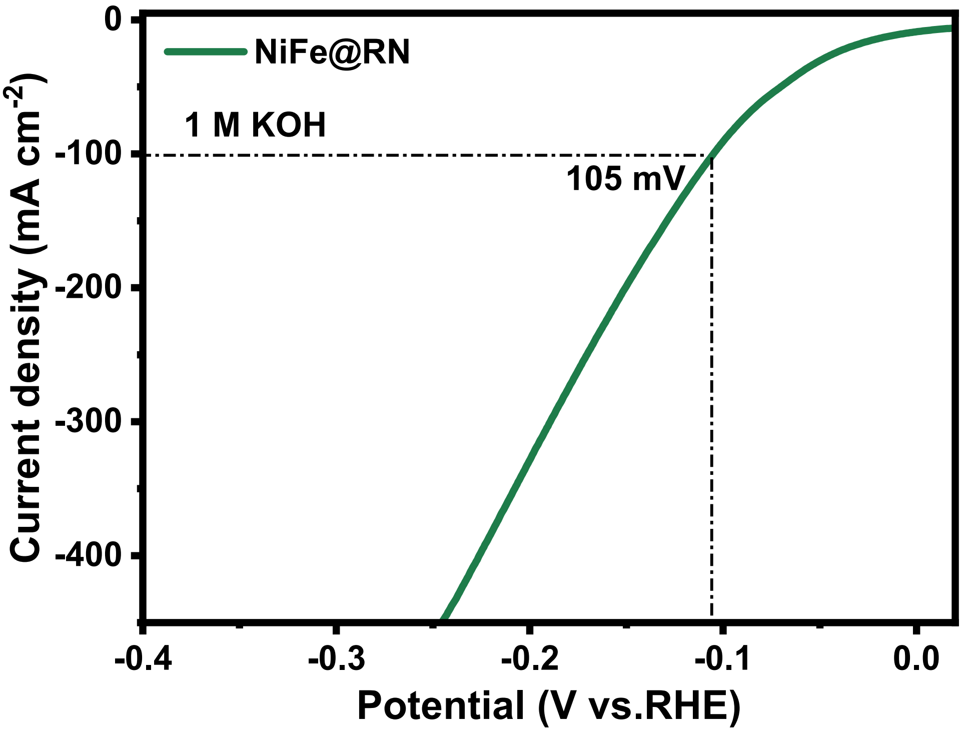

Fig. S19. LSV curve of NiFe@RN HER catalyst that tested in 1 M KOH solution.

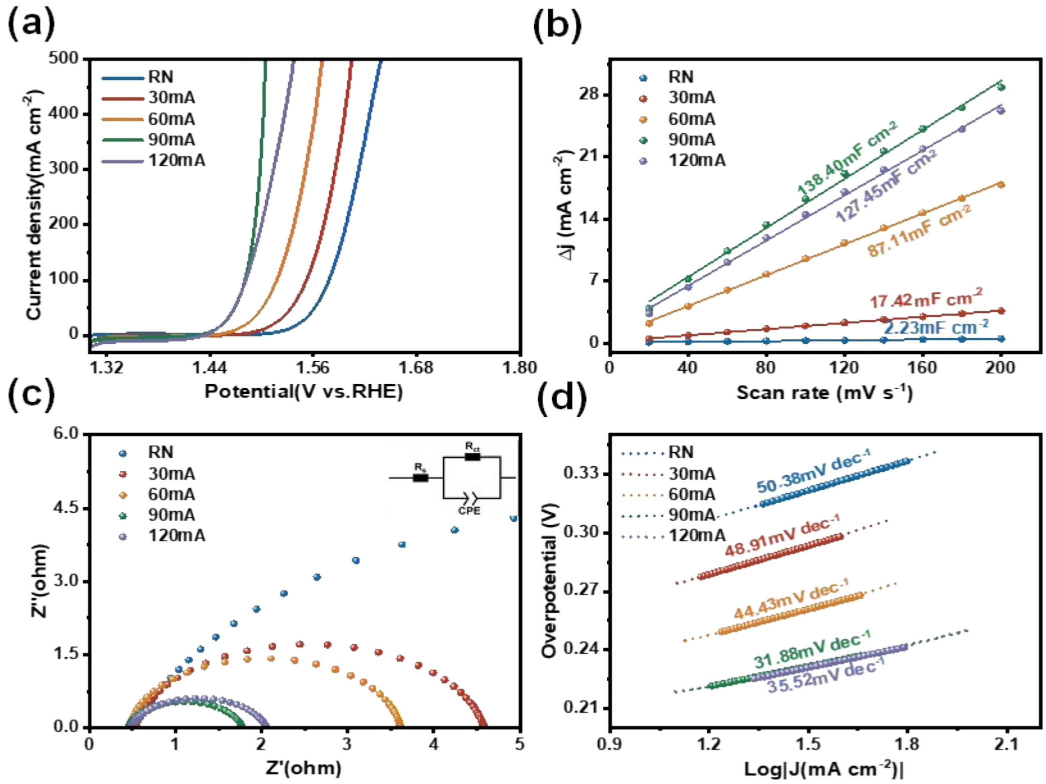

Fig. S20. (a) LSV curve of NiFe@RN OER catalyst that synthesizes at a different electrodeposition current in 6 M KOH solution, with a scanning rate of 1 mV s^{-1}; (b) Cdl calculation; (c) Electrochemical impedance spectroscopy (EIS) plots; (d) Tafel slope.

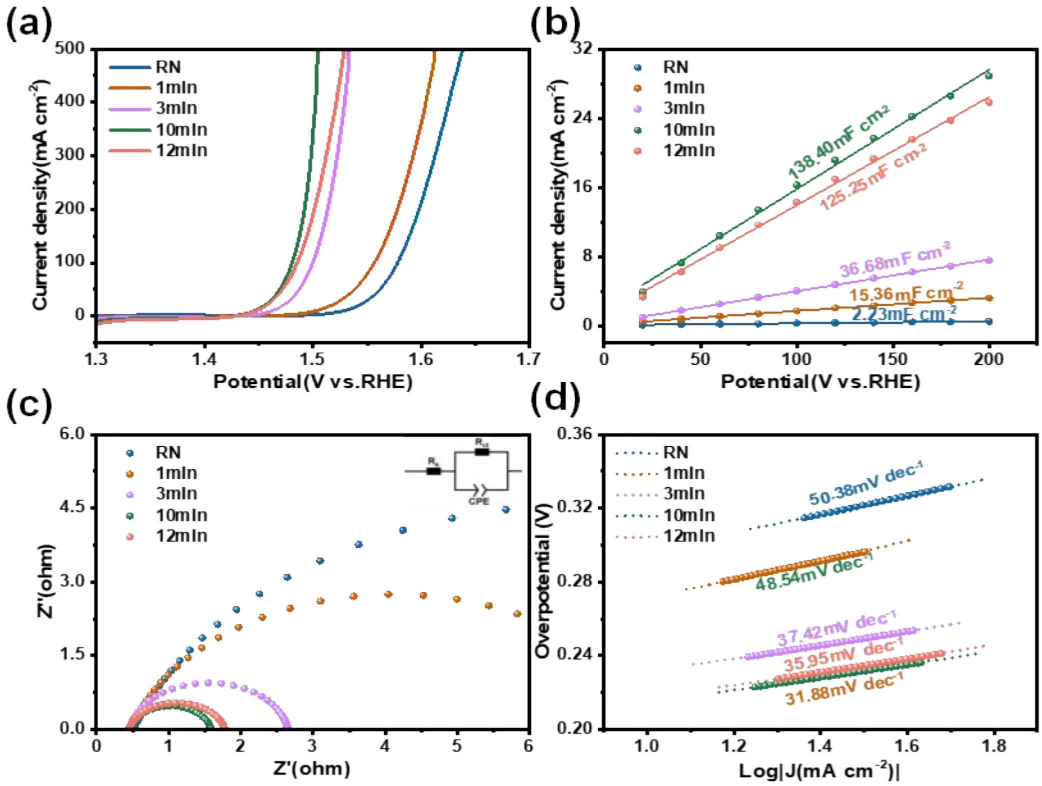

Fig. S21. (a) LSV curve of NiFe@RN OER catalyst that synthesizes at a different electrodeposition time in 6 M KOH solution, with a scanning rate of 1 mV s^{-1}; (b) Cdl calculation; (c) Electrochemical impedance spectroscopy (EIS) plots; (d) Tafel slope.

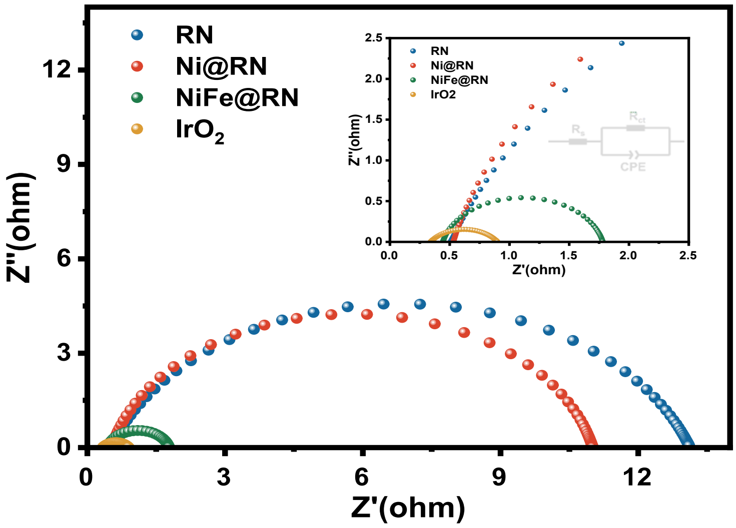

Fig S22. Nyquist plots of NiFe@RN and other catalysts.

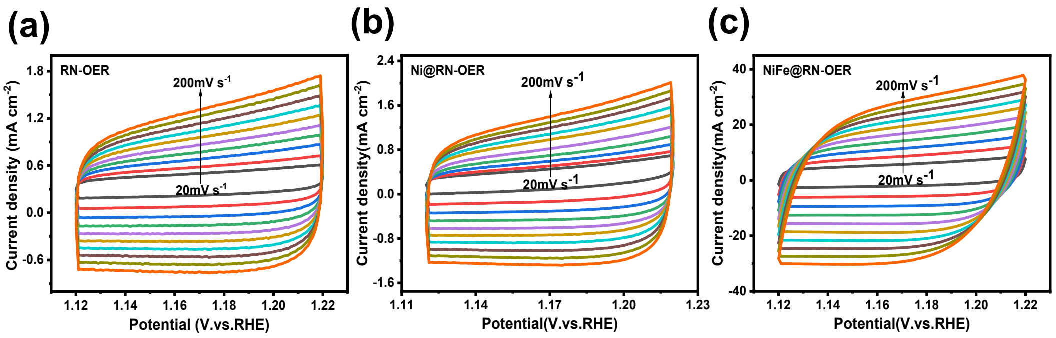

Fig S23. CV diagram (1.12-1.22 mV) of OER catalyst in 6 M KOH electrolyte. (a) RN; (b) Ni@RN and (c) NiFe@RN

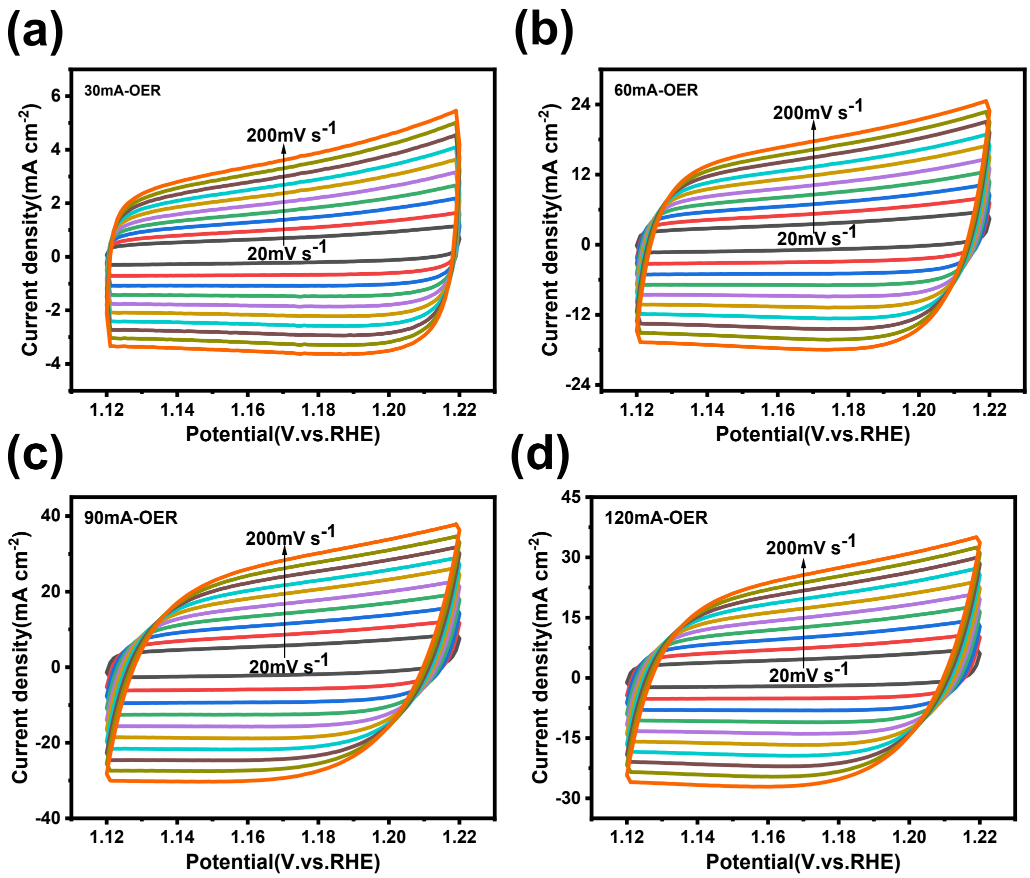

Fig S24. CV diagram (1.12-1.22 mV) of NiFe@RN OER catalyst that synthesizes at a different electrodeposition current. (a) 30 mA; (b) 60 mA; (c) 90 mA and (d) 120 mA.

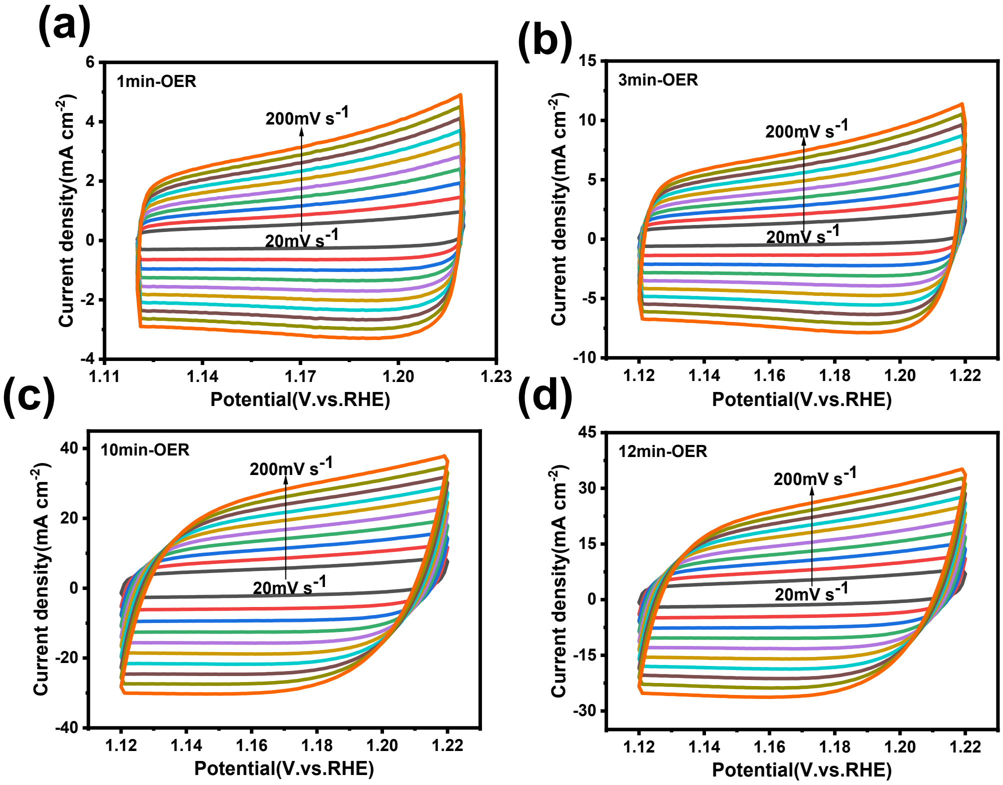

Fig S25. CV diagram (1.12-1.22 mV) of NiFe@RN OER catalyst that synthesizes at a different electrodeposition current. (a) 1 min; (b) 3 min; (c) 10 min and (d) 12 min.

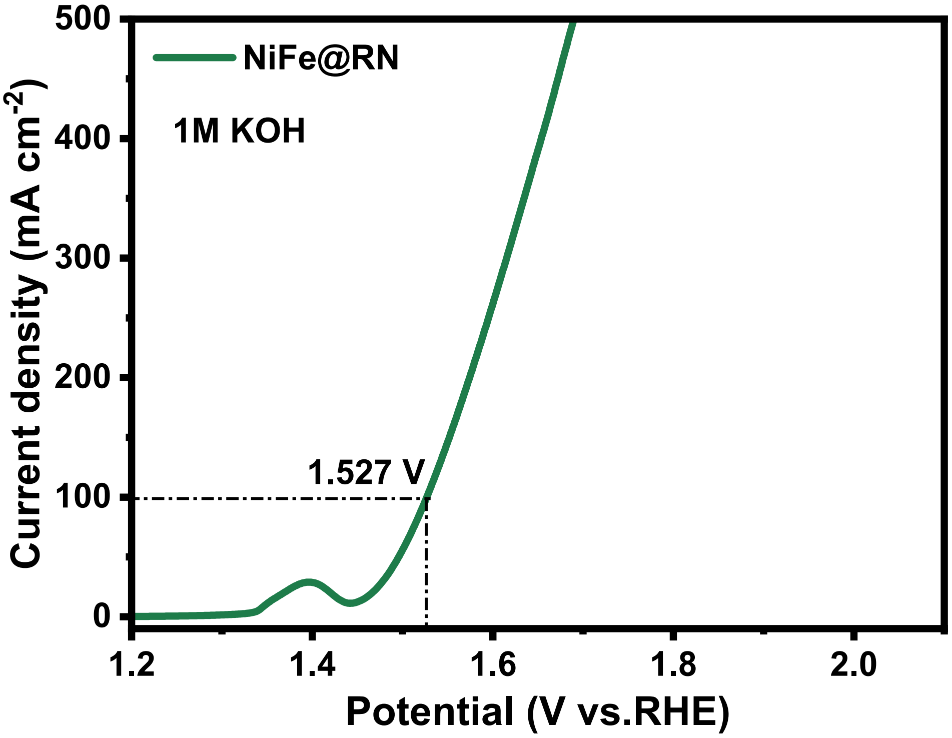

Fig. S26. LSV curve of NiFe@RN OER catalyst that tested in 1 M KOH solution.

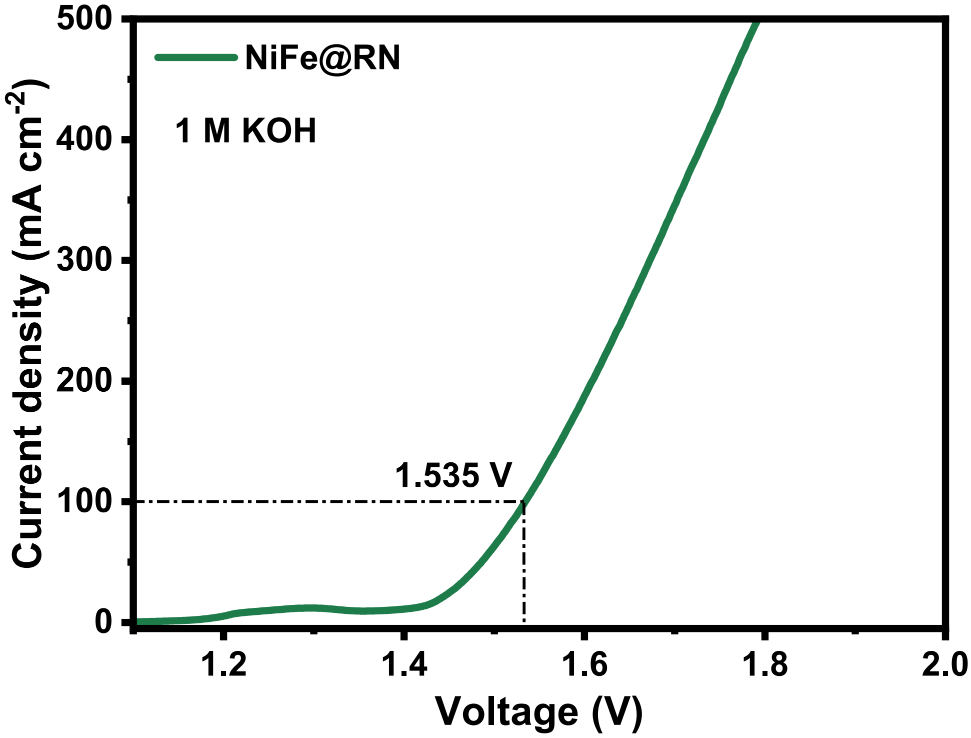

Fig S27. NiFe@RN cells in 1 M KOH electrolyte.

2. Supplementary Figures

Table S1. Elemental contents of different catalysts obtained from XPS measurement.

Catalyst	**Ni (At%)**	**Fe (At%)**	**O (At%)**
Ni@Raney Ni	23.61	/	41.36
NiFe@Raney Ni	19.04	3.7	39.73

Table S2. Elemental contents of different catalysts obtained from HRTEM measurement

Catalyst	Ni (At%)	Fe (At%)	O (At%)
NiFe@Raney Ni	58	7.8	34

Table S3. Charge Transfer Resistor Values of NiFe@RaneyNi、Ni@RN、Pt/C and IrO_2 catalysts

Name	**Rs (Ω)**	**Rct (Ω)**
NiFe@RN	0.4431	1.32
Ni@RN	0.531	11.01
Pt/C	0.4137	1.229
IrO_2	0.4324	1.47
RN	0.508	13.11
NF	0.3705	24.93

Table S4. Comparison of HER performance of NiFe@RN with bifunctional electrocatalysts reported in recent years

Electrocatalyst	Electrolyte	η(mV) @100 mA cm^{-2}	Tafel plots ($mV\ dec^{-1}$)	Reference
NiFe@RN	6 M KOH	93.51	32.74	This work
NiFe@RN	1 M KOH	105	-	This work
$Fe(OH)_x$-Ru/$Ni(OH)_2$	1 M KOH	127	43.2	[1]
NiFe LDHs-NiFe	1 M KOH	158	113.22	[2]
La-NMS@NF	1 M KOH	154	71	[3]
Co_2P/Ni_xP_y@NF	1 M KOH	155	86	[4]
CoMoP/CoP/NF	1 M KOH	127	44.5	[5]
Co_3O_4@NF	1 M KOH	224	109	[6]
$NiCo_2S_4$/NiFeP/NF	1 M KOH	205	99	[7]
Co/CoMoN/NF	1 M KOH	173	68.9	[8]
NiSe@NiFe-LDH/NF	1 M KOH	193	53.6	[9]
NiPS/NF	1 M KOH	169	89	[10]
$Ni_{12}P_5$-Fe_2P-NbP	1 M KOH	178	59	[11]
Ni/$Ni(OH)_2$	1 M KOH	153	46.8	[12]
FeCo-LDH/PANI	1 M KOH	246	115	[14]
Ni_3S_2	1 M KOH	127	67	[15]

Table S5. Comparison of OER performance of NiFe@RN with bifunctional electrocatalysts reported in recent years

Electrocatalyst	Electrolyte	η(mV) @ 100 mA cm^{-2}	Tafel plots ($mV\ dec^{-1}$)	Reference
NiFe@RN	6 M KOH	248	31.88	This work
NiFe@RN	1 M KOH	297	-	This work
$Fe(OH)_x$-Ru/$Ni(OH)_2$	1 M KOH	265	42.6	[1]
Ru-Ni(Fe)P_2/NF	1 M KOH	251	91.6	[16]
NiFe LDHs-NiFe	1 M KOH	268	64.29	[2]
Fe/Co/Ni-MoS_x/INF	1 M KOH	263	48.1	[17]
Co_2P/Ni_xP_y@NF	1 M KOH	300	158	[4]
La-NMS@NF	1 M KOH	300	152	[3]
CoMoP/CoP/NF	1 M KOH	308	72	[5]
$NiCo_2S_4$/NiFeP/NF	1 M KOH	293	110	[7]
Co/CoMoN/NF	1 M KOH	303	56	[8]
NiPS/NF	1 M KOH	320	23	[10]
NiFe LDH/FeOOH	1 M KOH	273.9	69.8	[18]
$NiFeO_xH_y$	1 M KOH	265	24	[19]
FeCo-LDH/PANI	1 M KOH	323	45	[14]
NiCoP@NiMn LDH/NF	1 M KOH	293	43.7	[20]

Table S6. Overall water splitting performance for NiFe@RanneyNi with other reported bifunctional electrocatalysts.

Electrocatalyst	Electrolyte	Voltages @ J($mAcm^{-2}$)	Reference
NiFe@RN	6 M KOH+80°C	1.49V@100	This work
NiFe@RN	1 M KOH+80°C	1.535V@100	This work
NiFe@NF	6 M KOH+80°C	1.56V@100	[21]
Ru-Ni(Fe)P_2/NF	1 M KOH	1.553@100	[16]
NiFe LDHs-NiFe	1 M KOH	1.703@100	[2]
MoS_2/Ni_3S_2@CA	1 M KOH	1.64@100	[22]
S-FeNi/NF ‖ S-FeNi/NF	1 M KOH	1.81@100	[23]
Pt/C ‖ IrO_2	1 M KOH	1.639@100	[24]
NiFeRu/C ‖ Ru, Fe-Ni_5P_4/C	1 M KOH	1.569@100	[24]
CNTs@NiP_2/NbP	1 M KOH	2.32@100	[25]
Ru-CMOP	1 M KOH	1.697@100	[26]
MoNiFe ‖ MoNiFe	1 M KOH	1.9@100	[27]
CoFeV-LDHs	1 M KOH	1.65V@100	[28]
Ni_3S_2/Cu-NiCo LDH	1 M KOH	1.75V@100	[29]
NiFe LDH/FeOOH	1 M KOH	1.81@100	[18]
IF-$NiCl_2$ ‖ IF-$NiCl_2$/$RuCl_3$	1 M KOH	1.60V@100	[30]
Co8FeV@CC	1 M KOH	1.65@100	[28]
NiFeOH/CoS_x/NF	1 M KOH	1.760@100	[31]
HP Ni-P	1 M KOH	1.686@100	[32]

Table S7. NiFe@RN Comparison of catalyst energy consumption with industrial operation

Electrocatalyst	Current density (mA cm^{-2})	100	200	300	400	500
NiFe@RaneyNi	Potential (V)	1.499	1.552	1.594	1.634	1.673
	Kw h/Nm^3 H_2	3.583	3.736	3.81	3.905	3.998
NiAl alloy	Potential (V)	1.77	1.86	1.95	2.02	2.09
	Kw h/Nm^3 H_2	4.24	4.45	4.68	4.84	5.00
NiAl powder	Potential (V)	1.68	1.78	1.88	1.94	2.00
	Kw h/Nm^3 H_2	4.01	4.26	4.49	4.65	4.79
NiCr alloy	Potential (V)	1.77	1.87	1.95	2.01	2.08
	Kw h/Nm^3 H_2	4.23	4.47	4.66	4.81	4.97

References

(1) Mo, Y.; Du, D.; Du, Y.; Feng, Y.; Tang, P.; Li, D. $Fe(OH)_x$ modified ultra-small Ru nanoparticles for highly efficient hydrogen evolution reaction and its application in water splitting. *Journal of Colloid and Interface Science* **2024**, *659*, 697-706. DOI: https://doi.org/10.1016/j.jcis.2024.01.018.

(2) Chen, Y.-F.; Li, J.-H.; Liu, T.-T.; You, S.-H.; Liu, P.; Li, F.-J.; Gao, M.-Q.; Chen, S.-G.; Zhang, F.-F. Constructing robust NiFe LDHs–NiFe alloy gradient hybrid bifunctional catalyst for overall water splitting: one-step electrodeposition and surface reconstruction. *Rare Metals* **2023**, *42* (7), 2272-2283. DOI: 10.1007/s12598-022-02249-x.

(3) Li, W.; Sun, Z.; Ge, R.; Li, J.; Li, Y.; Cairney, J. M.; Zheng, R.; Li, Y.; Li, S.; Li, Q.; Liu, B. Nanoarchitectonics of La-Doped Ni_3S_2/MoS_2 Hetetostructural Electrocatalysts for Water Electrolysis. *Small Structures* **2023**, *4* (11), 2300175. DOI: https://doi.org/10.1002/sstr.202300175 (acccessed 2024/03/25).

(4) Liu, H.; Zhang, Y.; Ge, R.; Cairney, J. M.; Zheng, R.; Khan, A.; Li, S.; Liu, B.; Dai, L.; Li, W. Tailoring the electronic structure of Ni_5P_4/Ni_2P catalyst by Co_2P for efficient overall water electrolysis. *Applied Energy* **2023**, *349*, 121582. DOI: https://doi.org/10.1016/j.apenergy.2023.121582.

(5) Wei, Y.; Li, W.; Li, D.; Yi, L.; Hu, W. Amorphous-crystalline cobalt-molybdenum bimetallic phosphide heterostructured nanosheets as Janus electrocatalyst for efficient water splitting. *International Journal of Hydrogen Energy* **2022**, *47* (12), 7783-7792. DOI: https://doi.org/10.1016/j.ijhydene.2021.12.106.

(6) Wang, J.; Yan, B.; Fang, B.; Jian, Z. Metal organic framework derived cobalt tetroxide for enhanced electrochemical hydrogen evolution reaction. *Materials Letters* **2023**, *332*, 133448. DOI: https://doi.org/10.1016/j.matlet.2022.133448.

(7) Jiang, J.; Li, F.; Su, H.; Gao, Y.; Li, N.; Ge, L. Flower-like $NiCo_2S_4$/NiFeP/NF composite material as an effective electrocatalyst with high overall water splitting performance. *Chinese Chemical Letters* **2022**, *33* (9), 4367-4374. DOI: https://doi.org/10.1016/j.cclet.2021.12.028.

(8) Ma, H.; Chen, Z.; Wang, Z.; Singh, C. V.; Jiang, Q. Interface Engineering of Co/CoMoN/NF Heterostructures for High-Performance Electrochemical Overall Water Splitting. *Advanced Science* **2022**, *9* (11), 2105313. DOI: https://doi.org/10.1002/advs.202105313 (acccessed 2024/03/25).

(9) Pan, Z.; Tang, Z.; Yaseen, M.; Zhan, Y. NiSe and Fe-Based Layerd Double Hydroxide Nanosheet/Ni Foam Bifunctional Catalyst for Water Splitting. *ACS Applied Nano Materials* **2022**, *5* (11), 16793-16803. DOI: 10.1021/acsanm.2c03764.

(10) Luo, L.; Xu, S.; Yu, X.; Wang, Z.; Li, W.; Du, Y.; Ruan, M.; Wu, Q. Vertically growing nanowall-like N-doped NiP/NF electrocatalysts for the oxygen evolution reaction. *Dalton Transactions* **2022**, *51* (26), 10160-10168, 10.1039/D2DT01494G. DOI: 10.1039/D2DT01494G.

(11) Wen, S.; Chen, G.; Chen, W.; Li, M.; Ouyang, B.; Wang, X.; Chen, D.; Gong, T.; Zhang, X.; Huang, J.; Ostrikov, K. Nb-doped layered FeNi phosphide nanosheets for highly efficient overall water splitting under high current densities. *Journal of Materials Chemistry A* **2021**, *9* (15), 9918-9926, 10.1039/D1TA00372K. DOI: 10.1039/D1TA00372K.

(12) Lai, W.; Ge, L.; Li, H.; Deng, Y.; Xu, B.; Ouyang, B.; Kan, E. In situ Raman spectroscopic study towards the growth and excellent HER catalysis of Ni/Ni(OH)$_2$ heterostructure. *International Journal of Hydrogen Energy* **2021**, *46* (53), 26861-26872. DOI: https://doi.org/10.1016/j.ijhydene.2021.05.158.

(13) Cao, D.; Dong, Y.; Tang, Y.; Ye, Y.; Hu, S.; Guo, Z.; Li, X. Amorphous Manganese–Cobalt Nanosheets as Efficient Catalysts for Hydrogen Evolution Reaction (HER). *Catalysis Surveys from Asia* **2021**, *25* (4), 437-444. DOI: 10.1007/s10563-021-09342-8.

(14) Han, X.; Lin, Z.; He, X.; Cui, L.; Lu, D. The construction of defective FeCo-LDHs by in-situ polyaniline curved strategy as a desirable bifunctional electrocatalyst for OER and HER. *International Journal of Hydrogen Energy* **2020**, *45* (51), 26989-26999. DOI: https://doi.org/10.1016/j.ijhydene.2020.07.006.

(15) Lv, X.; Kannan, P.; Ji, S.; Wang, X.; Wang, H. Synthesis of Ni_3S_2 catalysts using various sulphur sources and their HER and OER performances. *CrystEngComm* **2020**, *22* (39), 6517-6528, 10.1039/D0CE01015D. DOI: 10.1039/D0CE01015D.

(16) Wu, D.; Liu, B.; Li, R.; Chen, D.; Zeng, W.; Zhao, H.; Yao, Y.; Qin, R.; Yu, J.; Chen, L.; et al. Fe-Regulated Amorphous-Crystal Ni(Fe)P$_2$ Nanosheets Coupled with Ru Powerfully Drive Seawater Splitting at Large Current Density. *Small* **2023**, *19* (36), 2300030. DOI: https://doi.org/10.1002/smll.202300030 (acccessed 2024/03/25).

(17) Wang, C.; Zhang, J.; Wang, L.; Feng, J.; Wang, L.; Dong, L.; Long, C.; Li, D.; Hou, F.; Liang, J. Ternary transition metal of Fe/Co/Ni doping on MoS_x nanowires for highly efficient electrochemical oxygen evolution. *Sustainable Materials and Technologies* **2023**, *36*, e00645. DOI: https://doi.org/10.1016/j.susmat.2023.e00645.

(18) Jiang, K.; Liu, W.; Lai, W.; Wang, M.; Li, Q.; Wang, Z.; Yuan, J.; Deng, Y.; Bao, J.; Ji, H. NiFe Layered Double Hydroxide/FeOOH Heterostructure Nanosheets as an Efficient and Durable Bifunctional Electrocatalyst for Overall Seawater Splitting. *Inorganic Chemistry* **2021**, *60* (22), 17371-17378. DOI: 10.1021/acs.inorgchem.1c02903.

(19) Im, S. W.; Ahn, H.; Park, E. S.; Nam, K. T.; Lim, S. Y. Electrochemically Activated $NiFeO_xH_y$ for Enhanced Oxygen Evolution. *ACS Applied Energy Materials* **2021**, *4* (1), 595-601. DOI: 10.1021/acsaem.0c02476.

(20) Wang, P.; Qi, J.; Chen, X.; Li, C.; Li, W.; Wang, T.; Liang, C. Three-Dimensional Heterostructured NiCoP@NiMn-Layered Double Hydroxide Arrays Supported on Ni Foam as a Bifunctional Electrocatalyst for Overall Water Splitting. *ACS Applied Materials & Interfaces* **2020**, *12* (4), 4385-4395. DOI: 10.1021/acsami.9b15208.

(21) Feng, L.; Zhou, J.; Xiao, J.; Chen, F.; Zhao, Z.; Liu, M.; Zhang, N.; Gao, F. Simple cathodic deposition of FeS/NiS-activated Ni/NiO heterojunctions for high-concentration overall water splitting reactions. *International Journal of Hydrogen Energy* **2023**, *48* (77), 29852-29864. DOI: https://doi.org/10.1016/j.ijhydene.2023.04.077.

(22) Zhang, B.; Luo, H.; Ai, B.; Gou, Q.; Deng, J.; Wang, J.; Zheng, Y.; Xiao, J.; Li, M. Modulating Surface Electron Density of Heterointerface with Bio-Inspired Light-Trapping Nano-Structure to

Boost Kinetics of Overall Water Splitting. *Small* **2023**, *19* (3), 2205431. DOI: https://doi.org/10.1002/smll.202205431 (acccessed 2024/03/25).

(23) Feng, K.; Song, R.; Xu, J.; Chen, Y.; Lu, C.; Li, Y.; Hofer, W.; Lin, H.; Kang, Z.; Zhong, J. The S-Fe(Ni) sub-surface active sites for efficient and stable overall water splitting. *Applied Catalysis B: Environmental* **2023**, *325*, 122365. DOI: https://doi.org/10.1016/j.apcatb.2023.122365.

(24) Wang, Y.; Ye, Q.; Lin, L.; Zhao, Y.; Cheng, Y. NiFeRu/C and Ru, Fe-Ni_5P_4/C as complementary electrocatalyst for highly efficient overall water splitting. *Journal of Colloid and Interface Science* **2023**, *651*, 1008-1019. DOI: https://doi.org/10.1016/j.jcis.2023.08.014.

(25) Singh, S.; Nguyen, D. C.; Kim, N. H.; Lee, J. H. Interface engineering induced electrocatalytic behavior in core-shelled CNTs@NiP_2/NbP heterostructure for highly efficient overall water splitting. *Chemical Engineering Journal* **2022**, *442*, 136120. DOI: https://doi.org/10.1016/j.cej.2022.136120.

(26) Quan, Q.; Zhang, Y.; Wang, F.; Bu, X.; Wang, W.; Meng, Y.; Xie, P.; Chen, D.; Wang, W.; Li, D.; et al. Topochemical domain engineering to construct 2D mosaic heterostructure with internal electric field for high-performance overall water splitting. *Nano Energy* **2022**, *101*, 107566. DOI: https://doi.org/10.1016/j.nanoen.2022.107566.

(27) Gultom, N. S.; Chen, T.-S.; Silitonga, M. Z.; Kuo, D.-H. Overall water splitting realized by overall sputtering thin-film technology for a bifunctional MoNiFe electrode: A green technology for green hydrogen. *Applied Catalysis B: Environmental* **2023**, *322*, 122103. DOI: https://doi.org/10.1016/j.apcatb.2022.122103.

(28) Lv, J.; Liu, P.; Li, R.; Wang, L.; Zhang, K.; Zhou, P.; Huang, X.; Wang, G. Constructing accelerated charge transfer channels along V-Co-Fe via introduction of V into CoFe-layered double hydroxides for overall water splitting. *Applied Catalysis B: Environmental* **2021**, *298*, 120587. DOI: https://doi.org/10.1016/j.apcatb.2021.120587.

(29) Jia, L.; Du, G.; Han, D.; Hao, Y.; Zhao, W.; Fan, Y.; Su, Q.; Ding, S.; Xu, B. Ni_3S_2/Cu–NiCo LDH heterostructure nanosheet arrays on Ni foam for electrocatalytic overall water splitting. *Journal of Materials Chemistry A* **2021**, *9* (48), 27639-27650, 10.1039/D1TA08148A. DOI: 10.1039/D1TA08148A.

(30) Liu, X.; Guo, X.; Gong, M.; Zhao, T.; Zhang, J.; Zhu, Y.; Wang, D. Regulated iron corrosion towards fabricating large-area self-supporting electrodes for an efficient oxygen evolution reaction. *Journal of Materials Chemistry A* **2021**, *9* (40), 23188-23198, 10.1039/D1TA06370G. DOI: 10.1039/D1TA06370G.

(31) Bose, R.; Jothi, V. R.; Karuppasamy, K.; Alfantazi, A.; Yi, S. C. High performance multicomponent bifunctional catalysts for overall water splitting. *Journal of Materials Chemistry A* **2020**, *8* (27), 13795-13805, 10.1039/D0TA02697B. DOI: 10.1039/D0TA02697B.

(32) Song, D.; Hong, D.; Kwon, Y.; Kim, H.; Shin, J.; Lee, H. M.; Cho, E. Highly porous Ni–P electrode synthesized by an ultrafast electrodeposition process for efficient overall water electrolysis. *Journal of Materials Chemistry A* **2020**, *8* (24), 12069-12079, 10.1039/D0TA03739G. DOI: 10.1039/D0TA03739G.